Progress In Electromagnetics Research C, Vol. 112, 207–219, 2021

A High Isolation Multiband MIMO Antenna without Decoupling Structure for WLAN/WiMAX/5G Applications

Dhanasekaran Dileepan*, Somasundaram Natarajan, and Rengasamy Rajkumar

Abstract—In this paper, 1×1 and 2×2 Multiple-input Multiple-output (MIMO) antenna is designed for a multiband application. The antenna consists of three concentrated decagon-shaped rings which are responsible for obtaining the three resonance frequencies. The proposed antenna has a unique design technique; without using any decoupling structure the antenna attains better isolation performance. First, a two (1×1) element MIMO antenna with three different orientations (Orientation-I, II, and III) is studied. Second, a four-element MIMO antenna is designed without any decoupling structure for better performance. The above two antenna designs are fabricated and measured. The dimension of the proposed antenna element is 23.5 mm $\times$ 26.5 mm, and it has -10 dB impedance bandwidth over 2.4–2.52 GHz, 3.66–4 GHz, and 4.62–5.54 GHz, which cover various applications such as WLAN (2.4/5.2 GHz), WiMAX (2.5/5.5 GHz), public safety (4.9 GHz), and 5G (3.6–3.8 GHz). The proposed MIMO antenna diversity performances such as isolation, ECC, Directivity Gain, TARC, Channel Capacity Loss (CCL), and Mean Effective Gain (MEG) are studied.

1. INTRODUCTION

There is huge demand for multiple-input-multiple-output multiband antennas due to increased wireless systems that operate at a high-speed data rate, multipath property, and large channel capacity. MIMO antenna signal correlation should be low with good impedance characteristics, and individual elements possess high efficiency and isolation [1–3]. However, it is challenging to design antenna elements in a small, constrained space with high isolation, and there are various techniques [4–17] used by researchers to attain high isolation. In [4], a MIMO antenna with a dual-band resonance and a size of 74×47.3 mm^2 is designed for WLAN application. It has a small decoupling structure for isolation over 30 dB. In [5], three techniques, i.e., orientation, space between elements, and introduction of L-shaped strips in the DGS, are used to achieve the isolation of -17 dB. A frequency selective surface (FSS) based decoupling structure is used with a foldable monopole multiband MIMO antenna to realize better isolation [6]. A triple-band dielectric resonator MIMO antenna used open square slots in the edges to create decoupling between antennas [7]. In [8], the isolation of an inverted F-shaped MIMO antenna is enhanced by introducing an inverted T-slot and a meander line shorting in the ground plane. The meander line with a semicircular patch is designed for the WLAN application. It covers 2.4/5.2 GHz, and shorting meander line is employed between patches to enhance isolation around -25 dB [9].

A metamaterial-based 2×2 element MIMO L-shaped monopole antenna loaded with SRR for WLAN/WiMAX application is proposed for isolation enhancement [10]. A MIMO antenna with a compact structure for multiband application attains less than -27 dB isolation by using a defected ground structure and parasitic elements, which covers 2.4/5.2/5.8 GHz WLAN application, is proposed [11]. Mutual coupling value lower than -18 dB is obtained by introducing stepped cuts and elliptical

Received 26 March 2021, Accepted 10 May 2021, Scheduled 16 May 2021
* Corresponding author: Dhanasekaran Dileepan (dileepanphd@gmail.com).
The authors are with the Department of ECE, Vel Tech Rangarajan Dr. Sagunthala R&D Institute of Science and Technology, Chennai, India.

slots in the ground [12]. The dimension of the structure is $50 \times 50\,\text{mm}^2$ and covers 2.5/3.5/5.5 GHz WiMax applications. A dumbbell-shaped parasitic structure is employed between circular patch antenna elements to reduce mutual coupling less than $-25\,\text{dB}$ [13], where it can be used for C band applications. A compact two element dual-band MIMO antenna uses simple decoupling slots in the ground plane and helps to improve the isolation to less than 20 dB for the first resonance frequency [14]. A stub in the ground and in the feed line is introduced in a tri-band MIMO antenna for WLAN/WiMAX application to enhance isolation greater than 20 dB [15]. A slotted microstrip patch antenna is presented in [16] for WLAN/WiMAX application with dimension of $70 \times 60\,\text{mm}^2$, and simple slots are introduced between antenna elements to achieve an isolation of $-29\,\text{dB}$. Improvement of isolation between two elements is achieved by optimizing its orientation and spacing with an isolation of less than $-50\,\text{dB}$ in [17], $-15\,\text{dB}$ in [18], and $-24\,\text{dB}$ in [19].

Different MIMO antennas have been designed by using various techniques and listed in Table 1. Many of the reported antennas have low isolation, occupy a large size, and need a complex technique to obtain better isolation. The proposed antenna has certain advantages as 2×2 MIMO antenna elements are placed in a unique orthogonal orientation to realize high isolation. The orientation of the elements helps in avoiding the use of a complex decoupling structure. Similarly, the 1×1 MIMO antenna uses a simple orientation technique to achieve high isolation and expected Envelop Correlation Coefficient,

Table 1. Various MIMO antenna characteristics comparison.

Ref.	Antenna Size (mm)	Applications	Isolation method	Isolation (dB)	ECC	Frequency (GHz)
[4]	74×47.3	WLAN	Decoupling strucutre	$-20\,\text{dB}$	0.005	2.46–2.7, 5.04–5.5
[5]	50×50	WLAN/WiMAX	DGS with two MP lines	$-17.8\,\text{dB}$	0.011	2.09–2.86, 5.05–5.94
[7]	100×100	LTE	DRA slot	$-20\,\text{dB}$	0.02	1.63–1.84, 2.43–2.71, 3.27–3.75
[8]	52×77.5	WLAN	Inverted T slot in ground	$-15\,\text{dB}$	0.2	2.4–2.48, 5.15 to 5.825
[9]	60×60	WLAN	meandering-line	$-25\,\text{dB}$		2.4–2.48, 5.15–5.825
[10]	40×40	WLAN/WiMAX/5G	SRR	$-14\,\text{dB}$		2.4, 3.45, 5.5
[11]	50×30	WLAN	parasitic elements and DGS	$-24\,\text{dB}$	0.027	2.4–2.4835, 5.15–5.35, 5.725–5.875
[12]	50×50	WLAN/WiMAX	stepped slot ended with an ellipse in ground	$-18\,\text{dB}$	0.03	2.3–2.75, 3.4–3.75, 4.8–6.0
[13]	40×40	WiMAX/C-band	dumb-bell shaped slot	$-35\,\text{dB}$	0.005	3.10–3.19, 6.11–6.43, 7.50–8.04
[14]	25×24	WLAN	slots	$-20\,\text{dB}$	0.004	2.40–2.67, 5.46–5.73
[15]	37×38		Stub in ground and feed line	$-20\,\text{dB}$	0.05	2.1–2.7, 3.3–3.7, 4.9-5.35
[16]	70×60	WLAN and WiMAX	Ground slots	$-24.98\,\text{dB}$		2.37–2.42, 3.33–3.39
[17]	60×20	WLAN and Wi-Fi.	orientation	$-50\,\text{dB}$	0.0002	4.3–6.0
[18]	37×56	Bluetooth/C-band/ WLAN/WiMAX/Wi-Fi	DGS	$-15\,\text{dB}$	0.08	2.24–2.50, 3.60–3.99, 4.40–4.60, 5.71–5.90
[19]	65×21	WiFi/WiMAX/WLAN	Orientation	$-24\,\text{dB}$	0.001	2.22–2.54, 3.14–3.9, 5.3-5.7
Proposed antenna	23.5×83	WLAN/WiMAX/5G	Orientation	$-30.5\,\text{dB}$	0.001	2.4–2.52, 3.66–4, 4.62–5.52

Diversity Gain, Channel Capacity loss values in all operating frequencies. Simple antenna design and compact size is used to achieve multi-band resonance. Further, it provides a needed solution to modern wireless communications. In this paper, decagon ring-shaped two- and four-element MIMO antennas are introduced with compact size; isolation is enhanced without using any decoupling structure; and it exhibits multiband resonance covering 2.41–2.49 GHz (Bluetooth), 2.5/5.5 (WiMAX), 2.4/5.2 GHz (WLAN), 3.6–3.8 GHz (5G), and 4.9 GHz (public safety applications) applications.

2. ANTENNA DESIGN

The basic antenna structure is depicted in Figure 1 with its parameters and dimensions, and an FR4 substrate is used to print the antenna with a dielectric constant ($\varepsilon_r = 4.4$) and 1.6 mm as thickness. The initial antenna design with a single decagon ring resonates at 4 GHz and has radius of 4.8 mm, and to achieve multiband resonance additional rings of smaller dimensions are added inside the initial design. The addition of the second ring with radius of 3.6 mm enables a dual-band resonance at 2.5 GHz and 4.8 GHz. The third ring with radius of 2.4 mm creates a third resonance band at 3.8 GHz, and a slot in the ground improves the reflection coefficient value. The basic antenna's design evolution is shown in Figure 2, and optimized antenna parameters are represented in Table 2.

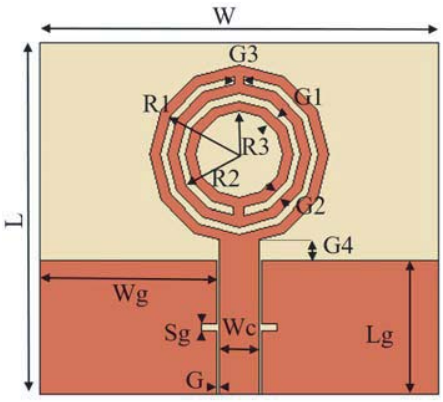

Figure 1. Basic antenna with parameters.

Figure 2. Basic antenna design evolution.

Table 2. Parameter of the antenna proposed.

Parameter	L	W	Wg	Lg	Wc	G	$G4$
Dimension (in mm)	23.5	26.5	11.75	9	2.6	0.2	1.6
Parameter	$G1$	$G2$, $G3$	$R1$	$R2$	$R3$	Sg	
Dimension (in mm)	0.7	0.5	4.8	3.6	2.4	0.5	

The conventional ring circular antenna can be designed using Equation (1) based on [20].

$$F = \frac{c}{\lambda} = \frac{c}{\pi(l_1 + l_2)\sqrt{\varepsilon_{eff}}} \text{ GHz} \tag{1}$$

with radius of the outer ring l_1 and radius of the inner ring l_2.

The proposed antenna S_{11} comparison is shown in Figure 3. As ring-2 and ring-3 are added to Antenna #1, mutual coupling between the rings is introduced and leads to producing the multiband response as illustrated in Figure 3. The antenna covers various frequencies such as 2.4/5.2 GHz, 2.5/5.5 GHz, and 4.9 GHz. The same designed antenna performance is validated with the measured result, as shown in Figure 4, and it is observed that there is a good agreement between them.

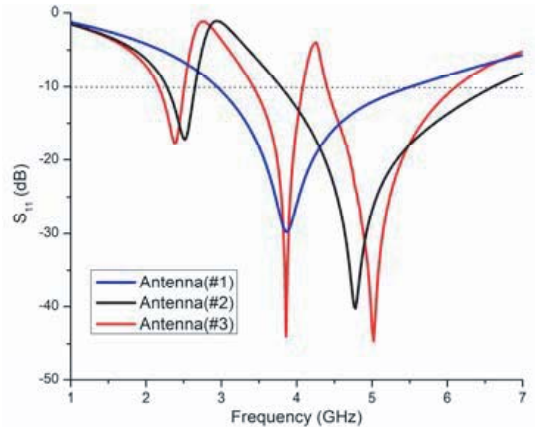

Figure 3. S_{11} comparison for various antenna design steps.

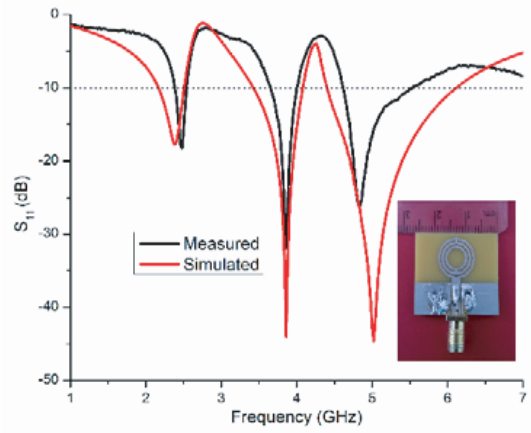

Figure 4. Simulated and measured S_{11} comparison.

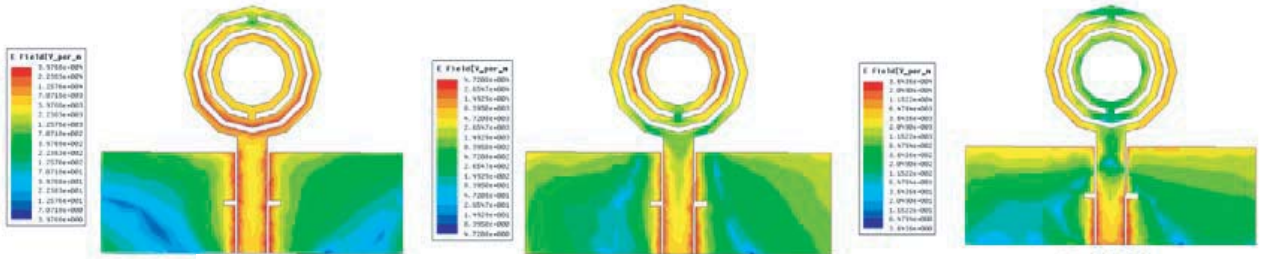

(a) 2.4 GHz (b) 3.8 GHz (c) 5.2 GHz

Figure 5. Current distribution of basic antenna.

The surface current distribution analysis of the proposed basic antenna for various operating frequencies is depicted in Figures 5(a)–(c). At 2.4 GHz, most of the current density can be seen between the inner edges of the outer ring and the outer edges of the middle ring. Current density states that the addition of the middle ring is accountable for the creation of resonance at 2.4 GHz due to coupling between them. Similarly, at 3.8 GHz current density is higher in the middle and inner rings, and the addition of a third smaller ring leads to the creation of a coupling effect between the middle and inner rings. Due to this coupling effect, a middle resonance frequency at 3.8 GHz is obtained. For 5.2 GHz, most of the current distribution is in the outer and middle rings. From the analysis of current distribution, it is evident that the addition of inner rings is responsible for multi-band resonance.

3. TWO ELEMENT MIMO ANTENNA DESIGN

The single element multi-band antenna geometry is depicted in Figure 1. It has a compact dimension of $23.5 \times 26.5\,\text{mm}^2$, and it resonates for three operating frequencies 2.4–2.52 GHz, 3.66–4 GHz, and 4.62–5.54 GHz. Two element MIMO antenna is studied for three different orientations, namely I, II, and III, as shown in Figures 6(a)–(c), and the separation between the elements is kept as 30 mm. Further, all three orientations are fabricated, and their S-parameter responses are illustrated in Figures 7–9.

Two element MIMO antenna (Orientation-I) is created by placing two antenna elements side by side with a separation of 30 mm, as shown in Figure 6(a). In this orientation, the antenna has a better reflection coefficient and isolation characteristics in all frequency bands. It is seen that the measured reflection coefficient for orientation-I is less than −15 dB in 2.4–2.5 GHz, 3.68–3.96 GHz, and 4.54–5 GHz. Similarly, the isolation values are −30.7 dB, −27.6 dB, and −18.5 dB for three frequency bands, and it is illustrated in Figure 7.

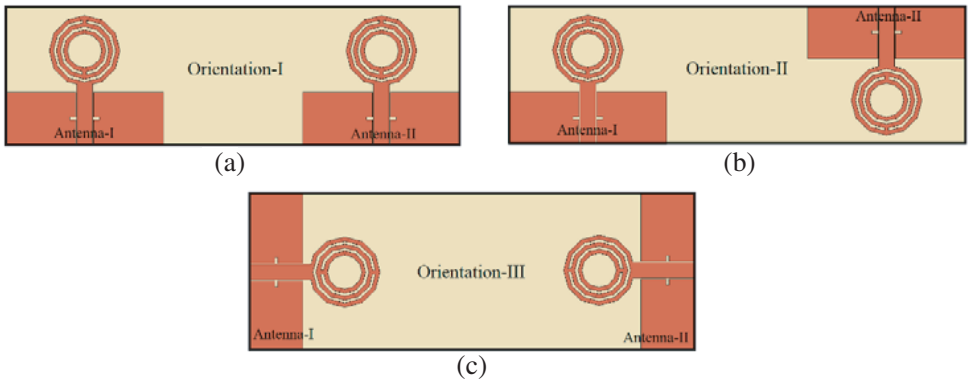

Figure 6. MIMO antenna with different orientation.

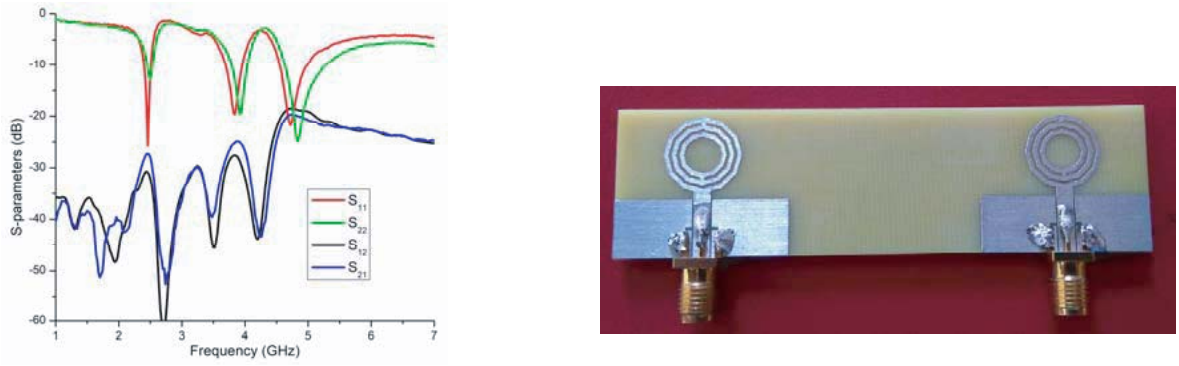

Figure 7. Measured S-parameters comparison and fabricated prototype of Orientation-I.

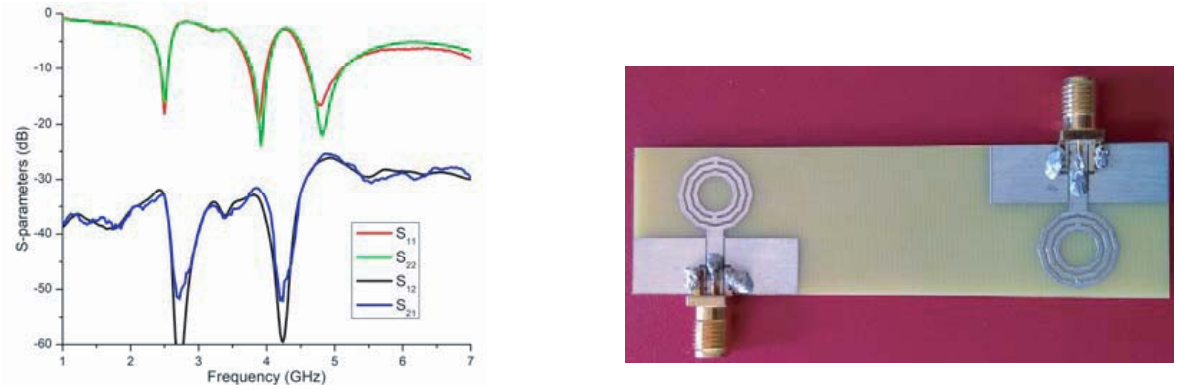

Figure 8. Measured S-parameters comparison and fabricated prototype of Orientation-II.

Orientation-II is created by inverting Antenna-II position where Antenna-I position is unchanged. For this orientation, the measured S-parameter response and fabricated prototype are shown in Figure 8. It is observed that it has covered 2.44–2.52 GHz, 3.8–4.06 GHz, and 4.64–5.32 GHz with isolation values less than −27.3 dB in the lower band, −24.9 dB in the middle band, and −19.7 dB in the higher band is observed.

Both Antenna-I and Antenna-II are rotated 90° to obtain the orientation-III as shown in Figure 6(c). In this orientation, the antenna radiating elements face each other.

Measured reflection coefficient of this antenna orientation covers 2.4–2.52 GHz, 3.66–4 GHz, and 4.62–5.54 GHz with an isolation value less than −30.5 dB in the lower band, −30.7 dB in the middle

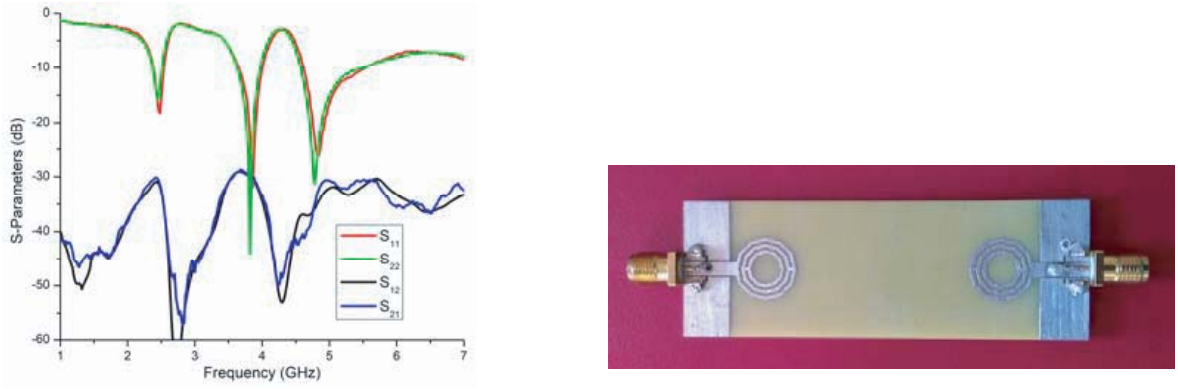

Figure 9. Measured S-parameters comparison and fabricated prototype of Orientation-III.

Figure 10. Two element MIMO antenna prototype with VNA measurement setup.

band, and -30.6 dB in the higher band being observed. Figure 9 presents measured S-parameter values of Orientation-III and its fabricated prototype. As per the above observations, MIMO antenna Orientation-III has a high isolation value of less than -30.5 dB in all operating frequencies compared to antenna Orientation-I and II. Figure 10 shows the two element MIMO antenna VNA measurement setup with the prototype.

4. TWO ELEMENT MIMO ANTENNA DIVERSITY PARAMETERS

The various MIMO antenna parameters like ECC (Envelop Correlation Coefficient), DG (Diversity Gain), TARC (Total Active Reflection Coefficient), MEG (Mean Effective Gain), and CCL (Channel Capacity Loss) are necessary for overall performance evaluation. MIMO antenna lower correlation coefficient value means that the antenna supports a higher data rate. ECC acceptable value for the practical condition is less than 0.5, and ECC for the proposed antenna is calculated using Equation (2) based on [22].

$$ECC_{(i,j,\ldots,N)} = \frac{\left|\sum_{n=1}^{N} S_{i,n}^{*} S_{n,j}\right|^{2}}{\prod_{k=i,j}\left[1 - \sum_{n=1}^{N} S_{k,n}^{*} S_{n,k}\right]} \tag{2}$$

where i and j are antennas 1 and 2, and N is the number of antennas.

Figure 11(a) shows the ECC graph of the proposed 1×1 MIMO antenna, where all operating frequencies has ECC value less than 0.5. Equation (3) represents the formula to calculate directivity gain (DG) using ECC. Diversity gain of the proposed 1×1 MIMO antenna is depicted in Figure 11(b) for all three operating frequencies, and it has a very desirable value of 10 dB.

$$DG = 10 \times \sqrt{1 - |ECC|} \tag{3}$$

TARC value for 1×1 MIMO antenna can be calculated using Equation (4), and it is shown in Figure 12(a). TARC is defined as the whole return loss value of MIMO antenna with the effect of mutual coupling and phase of incident wave [21].

$$TARC = \frac{\sqrt{(|S_{11} + S_{12}e^{j\theta}|)^2(|S_{21} + S_{22}e^{j\theta}|)^2}}{\sqrt{2}} \tag{4}$$

Mean Effective Gain (MEG) is the ratio of mean relative power received by the diversity antenna to the power incident on the isotropic antenna. Equations (5) and (6) can be used to calculate MEG, which depends on the S-parameter. MEG for the proposed two-element antenna is shown in Figure 12(b). As per observation the MEG value is less than -3 dB for all operating frequencies as expect in the MIMO

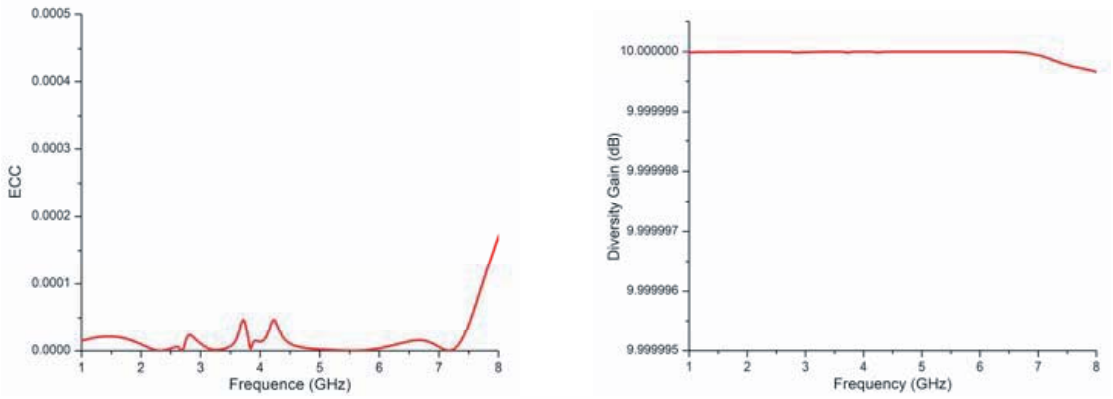

(a) (b)

Figure 11. (a) Envelop Correlation Coefficient (ECC) and (b) Diversity Gain (DG) of the proposed two element MIMO antenna.

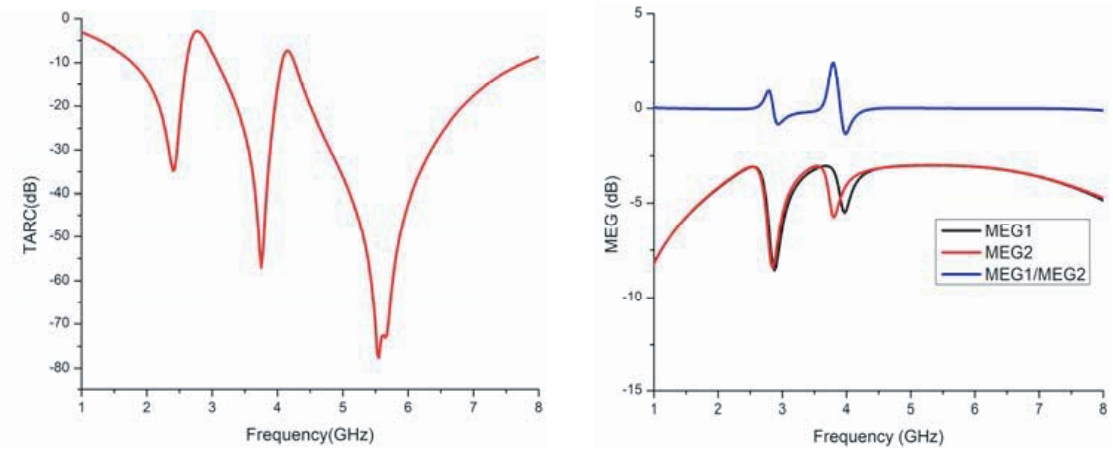

(a) (b)

Figure 12. (a) TARC and (b) MEG of the proposed two element MIMO antenna.

antenna.

$$MEG_1 = \frac{1}{2}[1 - |S_{11}|^2 - |S_{12}|^2] \tag{5}$$

$$MEG_2 = \frac{1}{2}[1 - |S_{21}|^2 - |S_{22}|^2] \tag{6}$$

As the number of antennas in a MIMO system increases, channel capacity will increase theoretically, but due to correlation, a capacity loss may be induced [19]. In Figure 13 Channel Capacity Loss is illustrated, where the CCL value less than 0.4 bits/sec/Hz is observed.

$$CCL = -\log_2(\rho^R) \tag{7}$$

$$\rho^R = \begin{pmatrix} \rho_{11} & \rho_{12} \\ \rho_{21} & \rho_{22} \end{pmatrix} \tag{8}$$

where,

$$\rho_{11} = 1 - (|S_{11}|^2 - |S_{12}|^2), \quad \rho_{22} = 1 - (|S_{22}|^2 - |S_{21}|^2),$$
$$\rho_{12} = -(S_{11}^* S_{12} + S_{21}^* S_{22}), \quad \rho_{21} = -(S_{22}^* S_{21} + S_{12}^* S_{11}).$$

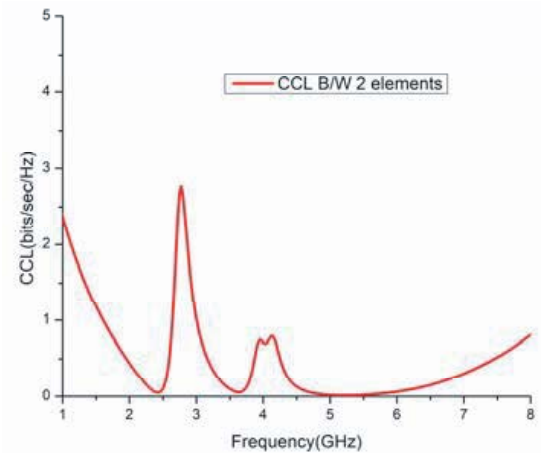

Figure 13. Channel capacity loss (CCL).

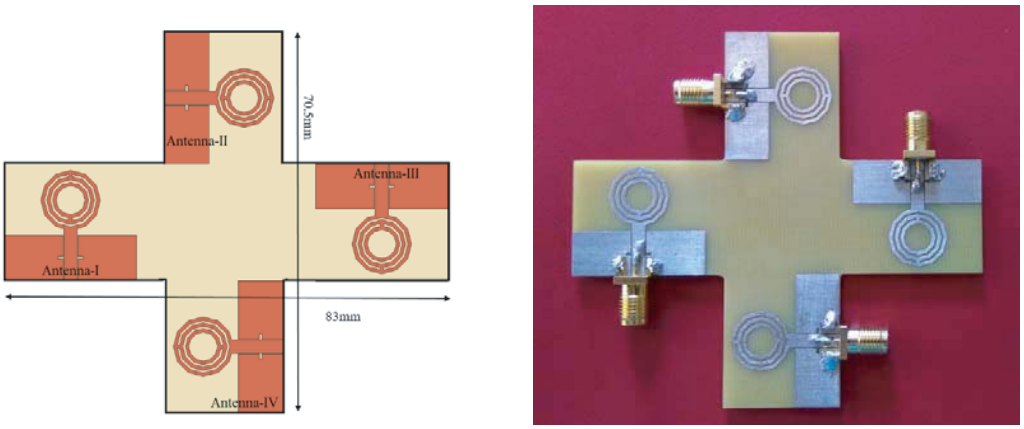

Figure 14. Four Port MIMO antenna configuration with the fabricated prototype.

5. FOUR ELEMENT MIMO ANTENNA DESIGN

Four element MIMO antenna is designed in a unique way, and each antenna is placed orthogonal to the nearer antenna to achieve high isolation. Figure 14 shows the four-element MIMO antenna configuration

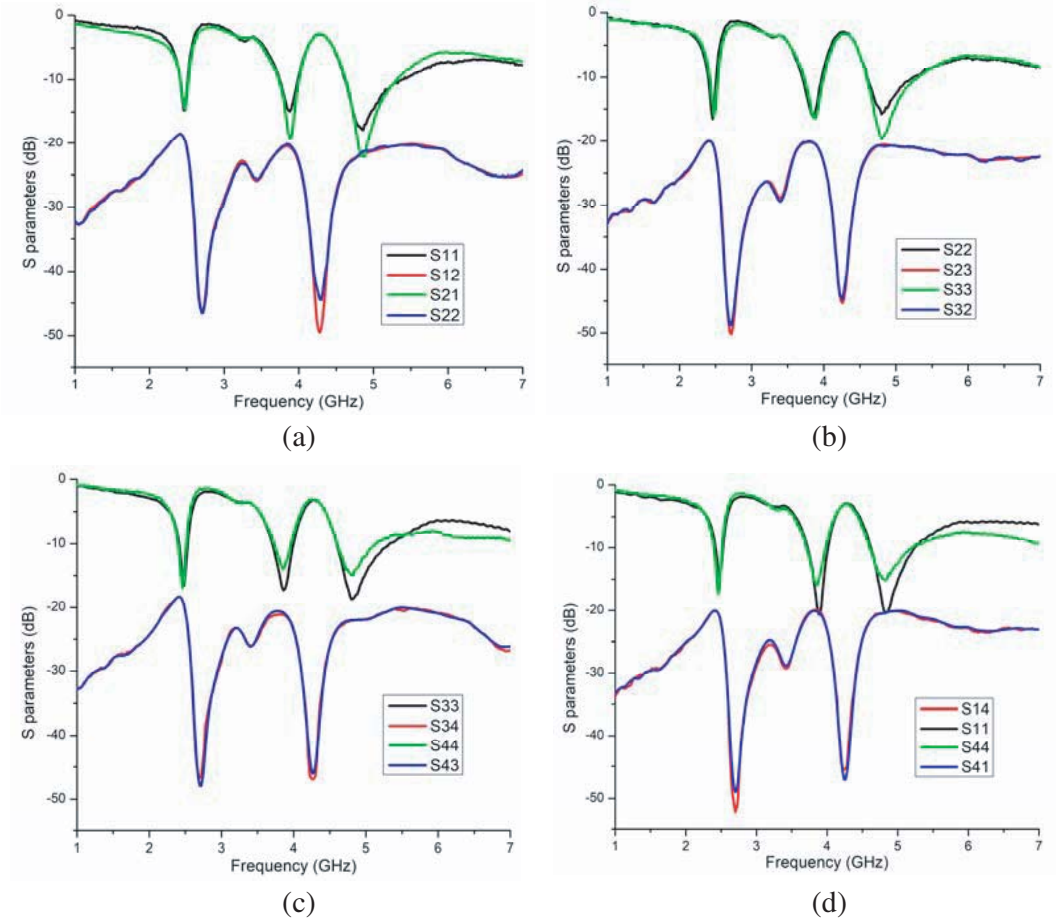

Figure 15. 2×2 MIMO antenna *S*-Parameter comparison. (a) Antenna-I and Antenna-II, (b) Antenna-II and Antenna-III, (c) Antenna-III and Antenna-IV, (d) Antenna-I and Antenna-IV.

Figure 16. Four element MIMO antenna prototype with VNA measurement setup.

and its fabricated prototype. S-parameter is measured for all four antennas, and their responses are illustrated in Figures 15(a)–(d). The isolation between antenna-I and antenna-II is obtained around −18.5 dB for all operating frequencies, as exhibited in Figure 15(a).

It is observed that Figure 15(b) has an isolation value of −20 dB between Antenna-II and Antenna-III. The isolation value between Antenna-III and Antenna-IV is less than −18.5 dB, as shown in Figure 15(c). Between Antenna-I and Antenna-IV the value is less than −20 dB, which is illustrated in Figure 15(d). From the above analysis, it is evident that the four-element antenna shows good isolation between antennas.

As the distance between the ports increases, the isolation of the antenna also increases, but the focus is to develop a compact MIMO antenna without using decoupling structures. The proposed antenna dimensions are used. Figure 16 depicts the proposed four element MIMO antenna prototype with a VNA measurement setup.

6. FOUR ELEMENT MIMO ANTENNA DIVERSITY PARAMETERS

Envelope Correlation Coefficient for four element MIMO antenna is calculated using Equation (2). Figure 17(a) depicts ECC of the proposed four element antenna where the value is less than 0.001. Diversity gain is shown in Figure 17(b) which is calculated from Equation (3). MEG is calculated between Antenna-I and Antenna-II and shown in Figure 18(a). Similarly, MEGs between Antenna-I and Antenna-III, and Antenna-II and Antenna-IV are depicted in Figures 18(b) and (c), respectively.

The proposed MIMO antenna radiation pattern is shown in Figure 19, wherein in all operating frequencies H-plane radiation pattern is omnidirectional, and in E plane dumbbell shape is observed.

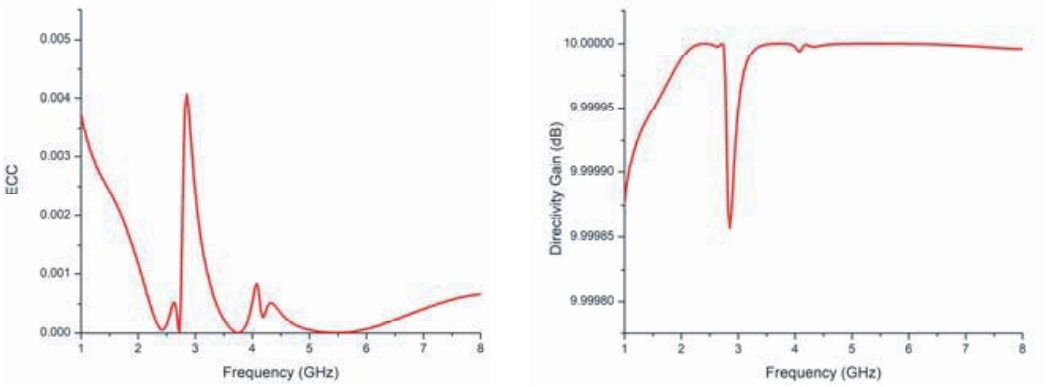

(a) (b)

Figure 17. (a) ECC of the proposed 2 × 2 MIMO antenna, (b) directivity Gain (DG) of the 2 × 2 MIMO antenna.

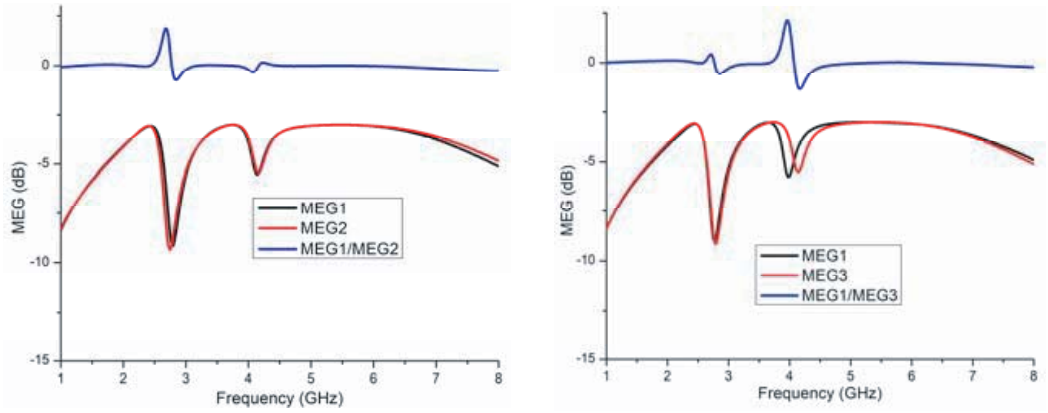

(a) (b)

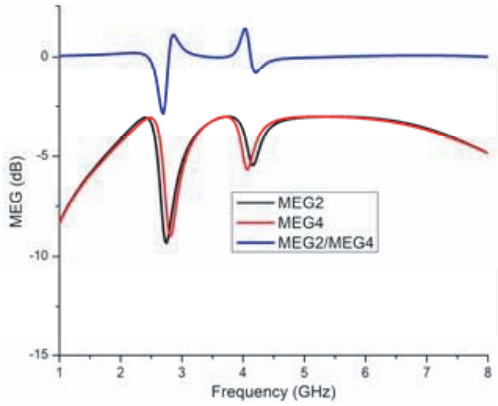

(c)

Figure 18. (a) MEG between Antenna-I and Antenna-II, (b) MEG between Antenna-I and Antenna-III and (c) MEG between Antenna-II and Antenna-IV of the proposed 2×2 MIMO antenna.

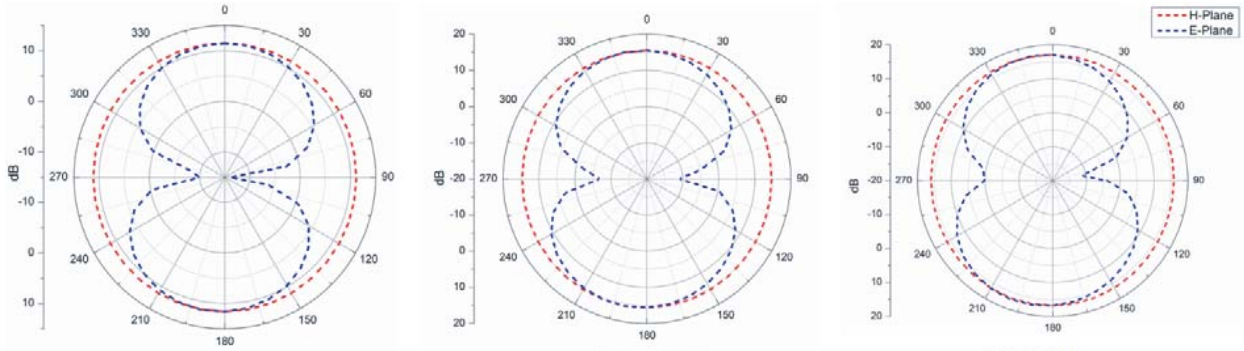

(a) 2.4 GHz (b) 3.8 GHz (c) 5.2 GHz

Figure 19. The proposed antenna E and H plane radiation pattern.

The proposed antenna has a positive gain over its operating frequencies, an average peak gain of 1 dB, and an efficiency is 85%.

7. CONCLUSION

In this paper, a multiband decagon ring-based 1×1 and 2×2 MIMO antenna without decoupling structure is presented. The proposed antenna's operating frequency bands are 2.4–2.52 GHz, 3.66–4 GHz, and 4.62–5.52 GHz, which cover 2.4/5.2 GHz WLAN, 2.5/5.5 GHz WiMAX, 3.6–3.8 GHz 5G, and 4.9 GHz public safety applications. The antenna element's orientation produces high isolation values of -30.5 dB and 18.5 dB for 1×1 and 2×2, respectively for all operating frequencies. The simulated efficiency of more than 85% and a stable radiation pattern are attained for the proposed antenna. MIMO antenna diversity performance is investigated, where measured results of the ECC values are lower than 0.001, and DG of 10 dB over operating frequencies is achieved. Thus the proposed MIMO antenna could be a good replacement for various modern wireless applications.

REFERENCES

1. Yang, Y., Q. Chu, and C. Mao, "Multiband MIMO antenna for GSM, DCS, and LTE indoor applications," *IEEE Antennas and Wireless Propagation Letters*, Vol. 15, 1573–1576, 2016, doi: 10.1109/LAWP.2016.2517188.

2. Ramachandran, A., S. Mathew, V. Rajan, and V. Kesavath, "A compact triband quad-element MIMO antenna using SRR ring for high isolation," *IEEE Antennas and Wireless Propagation Letters*, Vol. 16, 1409–1412, 2017, doi: 10.1109/LAWP.2016.2640305.
3. Sanmugasundaram, R., S. Natarajan, and R. Rajkumar, "A compact MIMO antenna with electromagnetic bandgap structure for isolation enhancement," *Progress In Electromagnetics Research C*, Vol. 107, 233–244, 2021.
4. Liu, P., D. Sun, P. Wang, and P. Gao, "Design of a dual-band MIMO antenna with high isolation for WLAN applications," *Progress In Electromagnetics Research Letters*, Vol. 74, 23–30, 2018.
5. Bai, J., R. Zhi, W. Wu, M. Shangguan, B. Wei, and G. Liu, "A novel multiband MIMO antenna for TD-LTE and WLAN applications," *Progress In Electromagnetics Research Letters*, Vol. 74, 131–136, 2018.
6. Saleem, R., M. Bilal, H. T. Chattha, S. Ur Rehman, A. Mushtaq, and M. F. Shafique, "An FSS based multiband MIMO system incorporating 3D antennas for WLAN/WiMAX/5G cellular and 5G Wi-Fi applications," *IEEE Access*, Vol. 7, 144732–144740, 2019, doi: 10.1109/ACCESS.2019.2945810.
7. Anuar, S. U., M. H. Jamaluddin, J. Din, K. Kamardin, M. H. Dahri, and I. H. Idris, "Triple band MIMO dielectric resonator antenna for LTE applications," *AEU — International Journal of Electronics and Communications*, Vol. 118, 153172, ISSN 1434-8411, 2020, https://doi.org/10.1016/j.aeue.2020.153172.
8. Deng, J., J. Li, L. Zhao, and L. Guo, "A dual-band inverted-F MIMO antenna with enhanced isolation for WLAN applications," *IEEE Antennas and Wireless Propagation Letters*, Vol. 16, 2270–2273, 2017, doi: 10.1109/LAWP.2017.2713986.
9. Deng, J. Y., Z. J. Wang, J. Y. Li, and L. X. Guo, "A dual-band MIMO antenna decoupled by a meandering line resonator for WLAN applications," *Microw. Opt. Technol. Lett.*, Vol. 60, 759–765, 2018, https://doi.org/10.1002/mop.31049.
10. Rajeshkumar, V. and R. Rajkumar, "SRR loaded compact tri-band MIMO antenna for WLAN/WiMAX applications," *Progress In Electromagnetics Research Letters*, Vol. 95, 43–53, 2021.
11. Wu, W., R. Zhi, Y. Chen, H. Li, Y. Tan, and G. Liu, "A compact multiband MIMO antenna for IEEE 802.11 a/b/g/n applications," *Progress In Electromagnetics Research Letters*, Vol. 84, 59–65, 2019.
12. Fang, Q., D. Mi, and Y.-Z. Yin, "A tri-band MIMO antenna for WLAN/WiMAX application," *Progress In Electromagnetics Research Letters*, Vol. 55, 75–80, 2015.
13. Babu, K. V. and B. Anuradha, "Analysis of multi-band circle MIMO antenna design for C-band applications," *Progress In Electromagnetics Research C*, Vol. 91, 185–196, 2019.
14. Nandi, S. and A. Mohan, "A compact dual-band MIMO slot antenna for WLAN applications," *IEEE Antennas and Wireless Propagation Letters*, Vol. 16, 2457–2460, 2017, doi: 10.1109/LAWP.2017.2723927.
15. Chaudhari, A. A. and R. K. Gupta, "A simple tri-band MIMO antenna using a single ground stub," *Progress In Electromagnetics Research C*, Vol. 86, 191–201, 2018.
16. Kommuri, R., "Isolation enhancement for dual-band MIMO antenna system using multiple slots loading technique," *Int. J. Commun. Syst.*, Vol. 33, e4470, 2020, https://doi.org/10.1002/dac.4470.
17. Mohammad Saadh, A. W., K. Ashwath, P. Ramaswamy, T. Ali, and J. Anguera, "A uniquely shaped MIMO antenna on FR4 material to enhance isolation and bandwidth for wireless applications," *AEU — International Journal of Electronics and Communications*, Vol. 123, 153316, ISSN 1434-8411, 2020, https://doi.org/10.1016/j.aeue.2020.153316.
18. Chouhan, S., D. K. Panda, V. S. Kushwah, and S. Singhal, "Spider-shaped fractal MIMO antenna for WLAN/WiMAX/Wi-Fi/Bluetooth/C-band applications," *AEU — International Journal of Electronics and Communications*, Vol. 110, 152871, ISSN 1434-8411, 2019, https://doi.org/10.1016/j.aeue.2019.152871.
19. Ekrami, H. and S. Jam, "A compact triple-band dual-element MIMO antenna with high port-to-port isolation for wireless applications," *AEU — International Journal of Electronics and Communications*, Vol. 96, 219–227, ISSN 1434-8411, 2018, https://doi.org/10.1016/j.aeue.2018.09.044.

20. Chen, X., G. Fu, S. Gong, Y. Yan, and W. Zhao, "Circularly polarized stacked annular-ring microstrip antenna with integrated feeding network for UHF RFID readers," *IEEE Antennas and Wireless Propagation Letters*, Vol. 9, 542–545, 2010, doi: 10.1109/LAWP.2010.2051791.
21. Chae, S. H., S. Oh, and S. Park, "Analysis of mutual coupling, correlations, and TARC in WiBro MIMO array antenna," *IEEE Antennas and Wireless Propagation Letters*, Vol. 6, 122–125, 2007, doi: 10.1109/LAWP.2007.893109.
22. Thaysen, J. and K. B. Jakobsen, "Envelope correlation in (N, N) MIMO antenna array from scattering parameters," *Microw. Opt. Technol. Lett.*, Vol. 48, 832–834, 2006, https://doi.org/10.1002/mop.21490.